Bulletin of the Seismological Society of America, Vol. 98, No. 6, pp. 2571–2589, December 2008, doi: 10.1785/0120080128

Regional Seismic Characteristics of the 9 October 2006 North Korean Nuclear Test

by Lian-Feng Zhao, Xiao-Bi Xie, Wei-Min Wang, and Zhen-Xing Yao

Abstract We investigate the regional seismic signature of the 9 October 2006 North Korean nuclear test. Broadband regional data for the nuclear test and a group of earthquakes close to the test site were obtained between December 2000 and November 2006. Epicentral distances from the stations to the test site are between 371 and 1153 km. We first use these regional events to calibrate the Lg-wave magnitude in the network. Then the network is used to calculate $m_b(Lg) = 3.93$ for the North Korean nuclear explosion. Using a modified fully coupled magnitude-yield relation, the yield of the North Korean nuclear test is estimated to be 0.48 kt. Because of large uncertainties in the source depth, the estimate is preliminary. The P/S-type spectral ratios Pg/Lg, Pn/Lg, and Pn/Sn are calculated for the nuclear explosion and a group of earthquakes close to the test site. At frequencies above 2 Hz, the network-averaged P/S spectral ratios clearly separate the 9 October 2006 explosion from the regional earthquakes. Our result indicates that a single-blast explosion in the North Korea region shows different seismic characteristics from an earthquake. Any well-coupled single-blast explosion detonated in this region with yield similar to that for the North Korean nuclear test has a large probability of being identified by a regional seismic network such as the one adopted in this study.

Introduction

Following the 9 October 2006 North Korean nuclear test, seismic signals were recorded at seismic networks around the world. The U.S. Geological Survey (USGS), National Earthquake Information Center (NEIC), Preliminary Determination of Epicenters (PDE) estimated its origin time to be 01:35:28.0 UTC. Its epicenter was 41.294° N and 129.094° E, and the source depth was nearly zero. Based on teleseismic data, the magnitude for this event is m_b 4.3. Based on this global body-wave magnitude and the fully coupled hard-rock magnitude-yield relation by Murphy (1996), the yield is approximately 0.6 kt (Kim and Richards, 2007).

For events of M 4 and smaller, the records from teleseismic distances are often weak and have low signal-to-noise ratios. It is difficult to extract reliable information from these data for investigating the details of sources. On the contrary, at epicentral distances between 200 and 2000 km, regional phases, for example, Pn, Sn, Pg, Lg, and Rg, can be clearly observed. These phases are sensitive to the source and the structure of the crust and uppermost mantle. They provide crucial information for investigating the features of small sources.

The continental crustal wave guide generally produces relatively small attenuation of the Lg wave, and the broad sampling of different ray paths from the source makes Lg particularly suitable for magnitude and yield estimation. Nuttli (1973, 1986a,b) developed a regional magnitude system based on the amplitude of the third peak in the Lg-wave train and created a relationship between the Lg-wave magnitude and explosion yield. Patton (1988) expanded Nuttli's method to a larger data set at the Nevada Test Site (NTS). Hansen *et al.* (1990) and Ringdal *et al.* (1992) found that magnitude estimation based on the root mean square (rms) amplitude of the Lg wave is very stable. A small number of stations can often give satisfactory estimates. Other researchers also confirmed that the rms amplitude measurements within the Lg group velocity window are very stable and accurate in magnitude and yield estimations (e.g., Israelsson, 1992; Priestley and Patton, 1997; Schlittenhardt, 2001). Patton and Schlittenhardt (2005) further developed Nuttli's method by linking the rms amplitude based Lg magnitude with the third peak amplitude based Lg magnitude.

On the other hand, various P/S-type amplitude ratios for high-frequency regional phases (e.g., Pn/Sn, Pn/Lg, Pg/Lg, and Pg/Sn) have become important for event discrimination. Taylor *et al.* (1989) investigated the discriminant performance of short-period spectral ratios between Pn, Pg, and Lg waves. Walter *et al.* (1995) found that both Pn/Lg and Pg/Lg ratios work better at higher frequencies. Fisk *et al.* (1996) compared Pn/Lg, Pn/Sn, and Pg/Lg ra-

tios and found that the explosions and earthquakes are well separated above 3 Hz but with considerable overlap below 2 Hz. Hartse *et al.* (1997) calculated phase, spectral, cross-spectral, short-period/long-period, and long-period ratios to test many possible event discriminants. Xie (2002) and Fisk (2006) scaled the regional *P*- and *S*-wave spectra models for explosions and earthquakes by adopting different corner frequencies for these waves. Based on this, they explained why the P/S ratio based discriminant is more efficient at high frequencies.

After the 9 October 2006 North Korean nuclear test, the regional seismic records from this event have been widely investigated for estimating its yield and for evaluating the discrimination capability in this region. To estimate the yield of the North Korean explosion, Herrmann *et al.* (2007) and Koper *et al.* (2008) calculated the seismic moment from the regional *Rg* wave recorded at stations MDJ and INCN. From the isotropic seismic moment, they calculated the explosion yield as a function of the source depth and the regional velocity model. By applying the Korean velocity model and using a reasonable depth range, their estimates of the yield vary between 0.25 and 2.0 kt. Salzberg and Marshall (2007) developed a semiempirical method that links seismic data from different events recorded at the same station. Based on this method and using a Chinese chemical explosion with known yield as a reference, they calibrated the seismic record of the North Korean explosion at station MDJ and estimated the yield as about 0.45 kt.

Kim and Richards (2007) and Richards and Kim (2007) investigated the spectral ratios generated by the North Korean explosion as well as by regional earthquakes and four known chemical explosions. They calculated the Pg/Lg spectral ratios for seismograms recorded at station MDJ. These spectral ratios overlapped significantly between frequencies of 1 and 7 Hz but were fairly well separated at 9 Hz and above. Koper *et al.* (2008) investigated amplitude ratios from filtered seismograms recorded at station MDJ for 18 regional events in North Korea and Northeast China, including the North Korean explosion and a group of earthquakes. They compared the amplitude ratios Pn/Lg and Pg/Lg for 1–4 Hz signals. They found the explosion always had the highest ratios, and the separation of the explosion from the earthquake population increased as the frequency increased. Walter *et al.* (2007) applied the magnitude and distance amplitude corrections to seismograms from the North Korean test and from a large group of earthquakes recorded at stations MDJ and TJN and calculated the Pg/Lg spectral ratios at 1–2, 2–4, 4–6, and 6–8 Hz. They found that the MDJ results discriminated the explosion and earthquakes at all frequencies above 2 Hz. The results from TJN showed partial overlap at low frequencies but discriminated well at frequencies of 6–8 Hz.

In this study, the digital broadband regional seismograms recorded by a network in Northeast China and South Korea are used to investigate the characteristics of the North Korean nuclear test. We use both Nuttli's (1986a) method based on the third peak and the method by Patton and Schlittenhardt (2005) based on the rms amplitude to calculate the regional magnitude. Then, the magnitude is used to estimate the yield of the North Korean explosion. We compare the characteristics of network-averaged P/S-type spectral ratios from both the explosion and a group of regional earthquakes. The potential capability of these spectral ratios as regional discriminants for separating explosions from earthquakes is investigated.

The Regional Data Set

Figure 1 shows the locations of the digital stations used in this study. The network is comprised of eight stations, in which, CN2, SNY, BNX, and DL2 are affiliated with China National Digital Seismic Network (CNDSN) and MDJ, INCN, BJT, and HIA are Global Seismic Network (GSN) stations. All stations are located in China except for INCN, which is located in South Korea. The parameters of these stations are listed in Table 1. The distances from these stations to the North Korean test site (NKTS) are between 371 and 1153 km, within which various types of regional phases are well developed and separated, with *Pn* to *Pg* interference at close range and upper mantle triplication at far regional distances being avoided. All CNDSN and GSN stations are equipped with broadband instruments that have nearly flat velocity responses between 0.03 and 8.0 Hz. The sampling rates of these instruments are listed in Table 1, and the frequency responses are illustrated in Figure 2. Also shown in this figure is the World-Wide Standard Seismogram Network (WWSSN) short-period (SP) response, which will be used

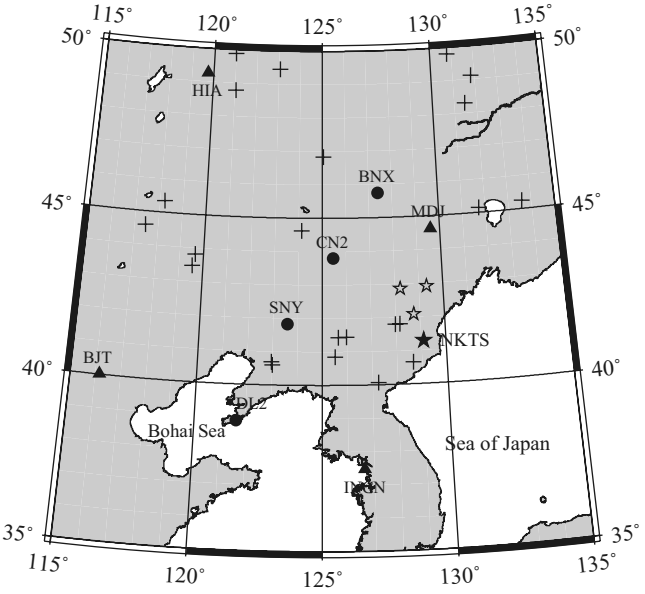

Figure 1. Map showing the locations of the NKTS (solid star) and the CNDSN (solid circles) and GSN (triangles) stations used in this study. Also illustrated in the figure are epicenters of earthquakes (crosses) that occurred between December 2000 and November 2006 and three chemical explosions (open stars) with known yields.

Table 1
List of Station Parameters Used in this Study

Number	Station	Latitude (°N)	Longitude (°E)	Elevation (m)	Distance (km)	Sampling Rate (sec^{-1})	Site Rock	Network
1	MDJ	44.616	129.592	200	371.6	40/20	Granite	GSN
2	CN2	43.801*	125.448*	223	411.9	50	Shale	CNDSN
3	SNY	41.828*	123.578*	54	467.9	50	Hybrid granite	CNDSN
4	INCN	37.483	126.633	419	475.4	40/20	Unknown	GSN
5	BNX	45.739*	127.405*	198	514.0	50	Granitic diorite	CNDSN
6	DL2	38.906*	121.628*	62	693.4	50	Quartzite	CNDSN
7	BJT	40.018	116.168	137	1106.2	20	Gravel	GSN
8	HIA	49.267	119.742	610	1152.6	20	Andesite	GSN

*From Ai *et al.* (2003).

for simulating the WWSSN SP seismograms for amplitude measurement.

Twenty-four regional seismic events, including the 9 October 2006 North Korean nuclear explosion and a group of nearby earthquakes, were recorded by this network between December 2000 and November 2006. In addition, there were three small chemical explosions, conducted in 1998 for seismic deep sounding purposes, recorded by the four GSN stations. The location of the NKTS and the epicenters of these earthquakes and chemical explosions are indicated in Figure 1. These vertical-component broadband recordings form the data set for calibrating the network and investigating the North Korean nuclear explosion.

Shown in Figure 3 are vertical-component broadband seismograms recorded by all eight stations for the North Korean nuclear explosion. The waveforms are normalized vertical ground velocities with station names, epicentral distances, and maximum amplitudes (in micrometers per second) listed on the left-hand side. The short bars on traces indicate group velocities. The seismograms recorded at distances less than 700 km show impulsive *P*-wave onset, which is the signature of an explosive source. For comparison, Figure 4 shows corresponding broadband seismograms from earthquake 20020416 which occurred on 16 April 2002 near the NKTS. Note that the earthquake has a weaker *P* wave and more prominent *S* waves.

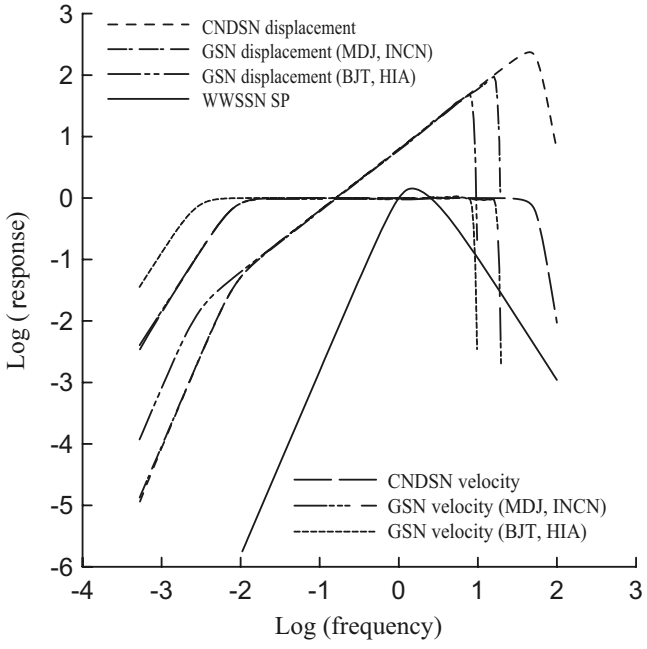

Figure 2. Instrument responses for CNDSN, Incorporated Research Institutions for Seismology (IRIS), and WWSSN SP stations.

Magnitude and Yield Estimation

Nuttli (1973, 1986a) and Patton and Schlittenhardt (2005) defined the regional magnitude $m_b(Lg)$ and created calibration coefficients to link the regional observations to the global body-wave magnitude, m_b,

$$m_b(Lg) = 5.0 + \log_{10}[A(10)/C], \quad (1)$$

where C is the Lg-wave amplitude caused by a m_b 5.0 event at a distance of 10 km and $A(10)$ is the assumed Lg-wave amplitude at a distance of 10 km caused by the event under estimation. Using proper geometrical spreading and attenuation models, we can extrapolate the observed Lg-wave amplitude at distance Δ to obtain $A(10)$. Based on the third peak method, Nuttli (1973, 1986a) obtained a C of 110 μm, which made the regional magnitude $m_b(Lg, TP)$ consistent with body-wave magnitude $m_b(P)$ in the central United States. Patton and Schlittenhardt (2005) obtained another C of 90 μm for rms amplitude based regional magnitude, $m_b(Lg, \text{rms})$.

Both Nuttli (1973, 1986a,b) and Patton and Schlittenhardt (2005) measured the Lg-wave amplitudes from WWSSN SP vertical-component seismograms. For broadband data, we first deconvolve the broadband instrument response from vertical-component seismograms and then convolve the seismograms with the WWSSN instrument response to simulate the WWSSN SP records. Shown in Figure 5 are simulated WWSSN seismograms from the North Korean explosion. Figure 6 shows a similar result for the earthquake 20020416. The traces have been normalized, and the station names, epicentral distances, and maximum amplitudes are listed in these figures. The short bars on the traces are different apparent group velocities. By visually checking the seismograms, we choose the Lg-wave group velocity windows to be between 3.5 and 2.9 km/sec for the explosion and be-

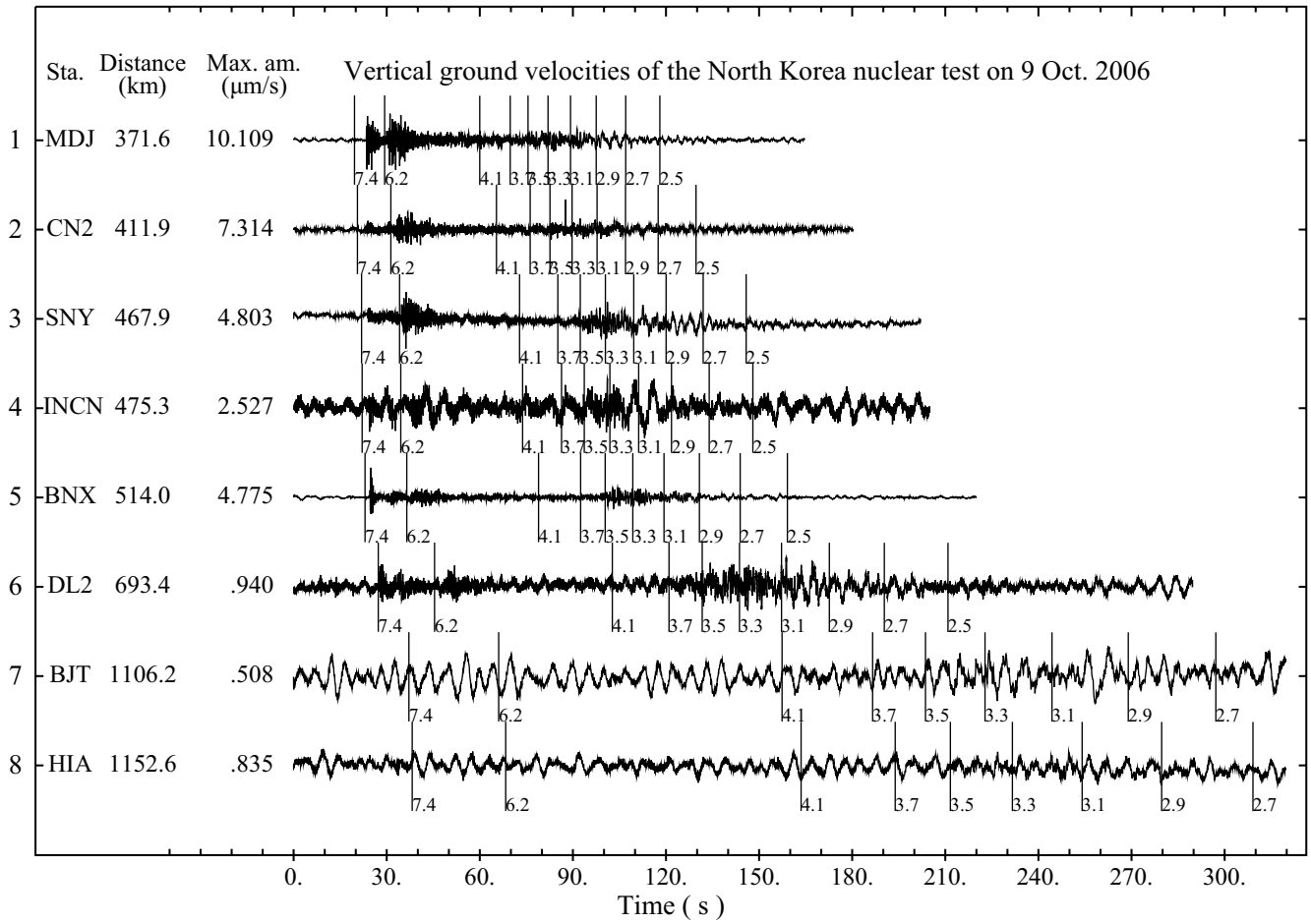

Figure 3. Observed seismograms for the North Korean nuclear test on 9 October 2006. The stations are ordered according to their epicentral distances, and the normalized vertical ground velocities are plotted. The station names and maximum amplitudes are listed on the left-hand side and are measured in micrometers per second. Marks on the waveforms indicate apparent group velocities.

tween 3.6 and 3.0 km/sec for the earthquake. These group velocities are slightly slower than the commonly used values between 3.6 and 3.2 km/sec, and the time windows are a little longer. The slightly different group velocities between the explosion and the earthquake may result from their different source depths, but the difference causes only a marginal effect on the result. Lg-wave amplitudes are measured using both the third peak method (Nuttli, 1973, 1980; Patton, 2001) and the rms method (Hansen *et al.*, 1990; Ringdal *et al.*, 1992).

Some stations have relatively large background noise. This is especially true for the two remote stations BJT and HIA (see Figs. 3 and 4). Noise correction is conducted to improve the quality of the rms amplitude measurements. Using the same method for measuring the data, we calculate the noise rms amplitude in a time window before the P-wave onset. The time window for noise measurement has the same length as the window for measuring the signal. Following Ringdal *et al.* (1992) and Schlittenhardt (2001), we assume that (1) the seismic record is a superposition of signal and noise, (2) the noise is stationary over a certain time period, and (3) the noise is uncorrelated with the signal. We then estimate the signal amplitude using $A_S^2 = A_R^2 - A_N^2$, where A_R and A_S are amplitudes of the raw data and the signal, respectively, and A_N is the noise amplitude from the pre-P time window. We do not consider the noise caused by the P coda.

To extrapolate the third peak amplitude $A(\Delta, TP)$ to the amplitude at reference distance $A(10, TP)$, we use the equation of Nuttli (1986a):

$$A(10, TP) = A(\Delta, TP)\left(\frac{\Delta}{10}\right)^{1/3}\left[\frac{\sin(\Delta/111.1)}{\sin(10/111.1)}\right]^{1/2}\exp[\gamma(\Delta - 10)], \quad (2)$$

where Δ is distance in kilometers, A is the amplitude in micrometers, and γ is the attenuation coefficient. At short epicentral distances (200–1200 km), the curvature of the Earth is negligible. Patton and Schlittenhardt (2005) used a slightly different equation to extrapolate the rms amplitude:

$$A(10, \text{rms}) = A(\Delta, \text{rms})\left(\frac{\Delta}{10}\right)^{1.0}\exp[\gamma(\Delta - 10)]. \quad (3)$$

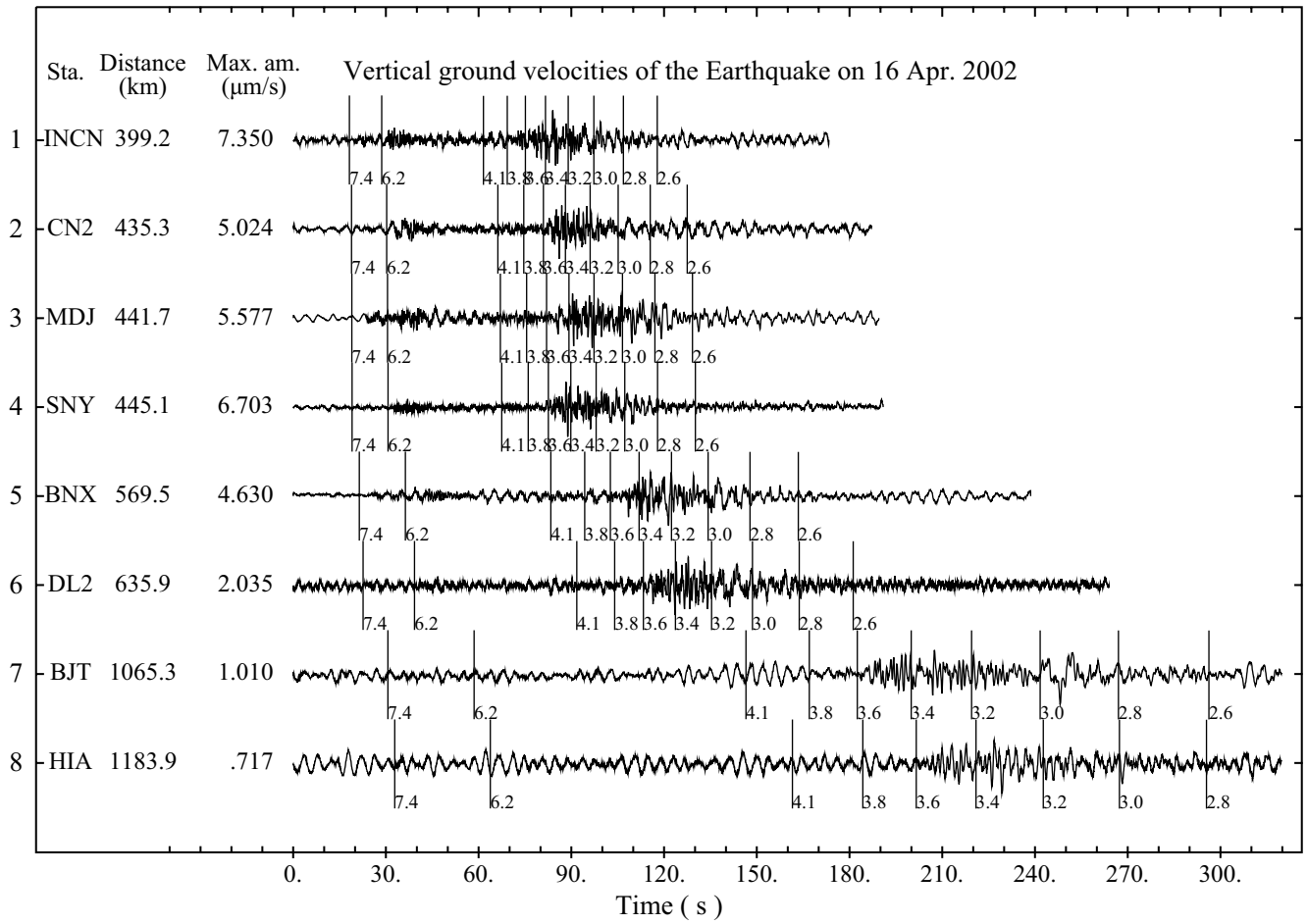

Figure 4. Similar to Figure 3, except these seismograms are for earthquake 20020416, which occurred near the NKTS on 16 April 2002.

Both equations (2) and (3) are crucially dependent on knowledge of the Lg attenuation coefficient γ around 1 Hz. Ge *et al.* (1989) investigated the Lg-wave attenuation in China and obtained a γ value of $2.7 \pm 0.4 \times 10^{-3}$ km^{-1} for Northeast China. Huang *et al.* (1990) used 21 regional events recorded on 27 stations to investigate the Lg-wave attenuation in Northeast China. By averaging both vertical and horizontal components, their result is 2.7×10^{-3} km^{-1}. If only the vertical component is considered, their result is 3.0×10^{-3} km^{-1}. These results are consistent with those obtained by Ge *et al.* (1989). The dominant frequencies used by these authors were approximately 1.5 Hz, and the average group velocity is 3.5 km/sec. Based on the relationship between the attenuation coefficient and the quality factor $\gamma(f) = \pi f / U(f) Q(f)$, where f is the frequency and U is the group velocity, the quality factors Q obtained by these authors are roughly between 450 and 500. Recently, based on the vertical-component Lg data in eastern Eurasia and using a dual station method, Xie *et al.* (2006) calculated the frequency dependent $Q(f) = Q_0 f^{\eta}$, where Q_0 is the 1 Hz Lg Q and η is a regional dependent power. In a region including Northeast China and the Korean Peninsula, they obtained Q_0 between 350 and 500 and η between -0.1 and 0.3. These results are consistent with those previously obtained by Ge *et al.* (1989) and Huang *et al.* (1990) but with higher accuracy and reliability. To calculate the Lg magnitudes, the average attenuation model $Q(f) = 420 f^{0.15}$ by Xie *et al.* (2006) is used.

To improve the accuracy of the magnitude measurement for the North Korean nuclear explosion, we use historical earthquakes in this region to calibrate the network. Twenty-four events including the nuclear explosion are used to calculate station corrections. The epicenters of these events are illustrated in Figure 1, and their parameters are listed in Table 2. We first calculate the Lg amplitude using both the third peak and the rms methods. These amplitudes are extrapolated to the reference distance using equations (2) and (3) and the attenuation model by Xie *et al.* (2006). Following the original definition of Nuttli (1973), we determine the frequencies by counting the number of zero-crossings. The amplitudes $A(10, TP)$ and $A(10, \text{rms})$ are used to calculate Lg magnitudes $m_b(Lg, TP)$ and $m_b(Lg, \text{rms})$ for all 24 events at all stations. The network-averaged magnitudes along with their standard deviations are then calculated and listed in Ta-

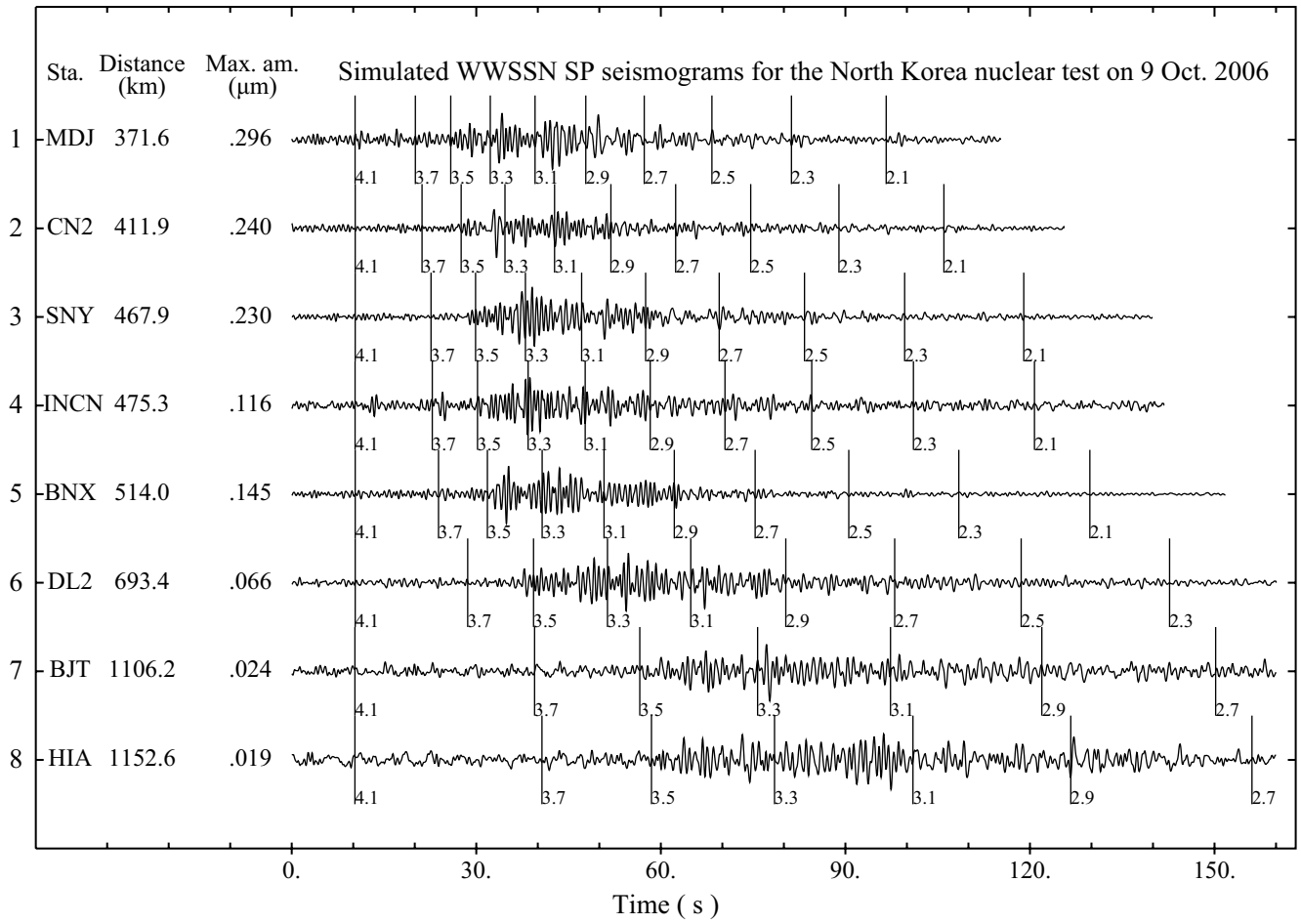

Figure 5. Simulated WWSSN SP vertical-component seismograms for the North Korean nuclear explosion. The maximum amplitudes and the group velocities are illustrated in the figure.

ble 2. Also listed in Table 2 are body-wave magnitudes, m_b, and local magnitudes, M_L, reported by ISC, NEIC, BJI (Beijing regional network), and SKHL (Sakhalin regional network). Next, the differences between the station magnitudes and the network-averaged magnitudes are calculated for each station. We then average these differences at each station to obtain the station corrections that are listed in Table 3. Finally, these station corrections are used for correcting the magnitude of the North Korean nuclear explosion. Listed in Table 4 are station names and Lg-wave amplitudes and magnitudes from individual stations for the North Korean nuclear explosion. The network-averaged values $m_b(Lg, TP)$ 3.93 and $m_b(Lg, \text{rms})$ 3.93 are also listed in the table.

Nuttli (1973, 1986a) built the Lg-wave magnitude by linking the Lg-wave magnitude, $m_b(Lg)$, to the body-wave magnitude, $m_b(P)$. We compare the Lg-wave magnitudes obtained here with the body-wave magnitudes, $m_b(P)$, and local magnitudes, M_L, for the same group of events to check the quality of measurement. Shown in Figure 7a is $m_b(Lg)$ versus the body-wave magnitude $m_b(P)$, and Figure 7b is $m_b(Lg)$ versus the local magnitude M_L, where crosses denote $m_b(Lg, TP)$ and diamonds denote $m_b(Lg, \text{rms})$. The empirical relationships from the least-squares fitting (solid lines in Fig. 7a and b) are

$$m_b(Lg) = (0.0250 \pm 0.2596) + (1.0051 \pm 0.0656) m_b(P), \tag{4a}$$

$$m_b(Lg) = (-0.7956 \pm 0.2198) + (1.1163 \pm 0.0459) M_L, \tag{4b}$$

where the numbers following the $\pm$ signs are standard deviations. Because the values of $m_b(Lg, TP)$ and $m_b(Lg, \text{rms})$ are very close, we do not separate them in these linear regressions. In equation (4), the slopes are close to unity. If we restrict the slope to 1.0, these relationships (dashed lines in Fig. 7a and b) become

$$m_b(Lg) = (0.0624 \pm 0.2444) + m_b(P), \tag{5a}$$

$$m_b(Lg) = (-0.2633 \pm 0.1809) + M_L. \tag{5b}$$

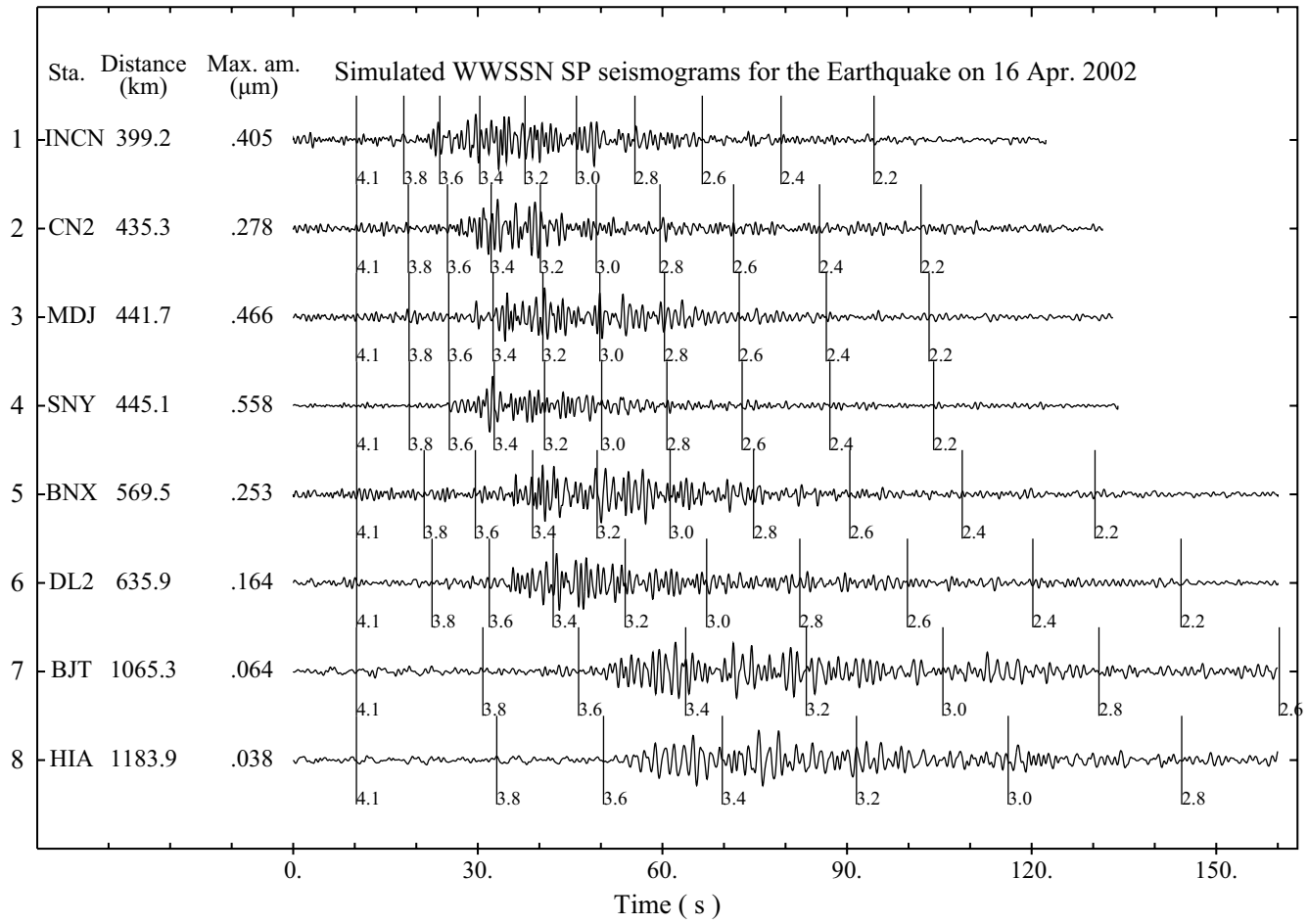

Figure 6. Similar to Figure 5, except the seismograms are for earthquake 20020416, which occurred on 16 April 2002 near the NKTS.

From equation (5a), there is a systematic difference of 0.06 magnitude unit between the $m_b(Lg)$ and $m_b(P)$ measurements. From equation (5b), the difference between the $m_b(Lg)$ and M_L is -0.26 magnitude unit. The difference between the $m_b(P)$ and M_L is about -0.3 magnitude unit. The local magnitude M_L is usually reported by regional networks for smaller earthquakes. Because of the regional geological variations and different equations used for M_L measurements, systematic variations may exist between these M_L reports. These effects are neglected in this study.

These relationships are similar to those reported by Nuttli (1986b) for central Asia. The differences between the slopes and intersections may come from the different magnitude populations used. When compared to the magnitude range between 5.3 and 6.2 used by Nuttli (1986b), most of the events used in this study are smaller or low-yield events. Figure 7a and b and equations (4) and (5) show that the Lg-wave magnitudes obtained here are consistent with the body-wave magnitude $m_b(P)$, indicating that the attenuation correction and station correction in data processing are properly treated. Figure 7c compares Lg magnitudes calculated using the third peak method and rms amplitudes. The least-squares fitting gives

$$m_b(Lg, \text{rms}) = (0.0090 \pm 0.0258) + m_b(Lg, TP), \quad (6)$$

demonstrating that these two methods give very similar results.

Nuttli (1986a) developed a method for determining the yield of underground nuclear explosions from Lg-wave observations. Using the recorded NTS explosions with announced yields, he calibrated the empirical $m_b(Lg)$-yield relationships for unsaturated and water-saturated site conditions. The equation for saturated material

$$m_b(Lg) = 3.943 + 1.124 \log Y - 0.0829(\log Y)^2, \quad (7)$$

where Y is the yield in kilotons, was found to provide reasonably accurate yield estimates for explosions in other areas of the United States and in the French Sahara. Nuttli (1986a) also suggested that it may be applicable to all continental areas. Nuttli (1986b) used this relationship to estimate the yields of the explosions at the East Kazakhstan test site. Ringdal *et al.* (1992) investigated the seismic yield for Soviet underground nuclear explosions at the Shagan River test site. Murphy (1996) investigated a group of Soviet nuclear tests and the peaceful nuclear explosions detonated in different geological materials. Both authors suggested that the ap-

Table 2

Events Used for Station Corrections

	Epicentral Parameters					Magnitude		$m_b(Lg, TP)$			$m_b(Lg, \text{rms})$		
Contributor	Date (yyyy/mm/dd)	Time (UTC)	Latitude (°N)	Longitude (°E)	Depth (km)	m_b	M_L	Stations*	Average	Standard Deviation	Stations*	Average	Standard Deviation
BJI†	2000/12/13	09:59:31.20	40.850	125.530	27.0	—	3.3	5	3.04	0.22	5	2.99	0.22
ISC	2002/04/16	22:52:38.63	40.658	128.652	10.0	4.1	4.5	8	4.19	0.11	8	4.19	0.11
ISC	2002/04/30	03:22:43.56	40.692	122.964	15.0	3.7	4.1	8	4.00	0.22	8	3.99	0.20
BJI	2002/05/05	10:02:24.90	40.060	127.240	15.0	—	3.4	8	2.97	0.18	8	2.92	0.26
ISC	2002/06/16	21:58:40.16	40.601	123.007	33.0	3.9	4.0	8	3.93	0.18	8	3.94	0.21
ISC	2002/08/29	18:32:16.26	49.451	123.067	16.0	3.6	4.3	8	3.95	0.31	8	3.94	0.30
ISC	2002/10/20	15:46:19.95	44.600	117.469	33.0	4.8	5.2	7	5.00	0.14	7	5.02	0.12
BJI	2002/11/25	11:19:38.00	41.800	128.170	13.0	—	3.0	5	2.59	0.25	4	2.60	0.26
ISC	2003/06/01	02:49:17.28	49.800	130.793	7.0	4.0	3.9	7	4.02	0.18	7	4.01	0.17
SKHL‡	2003/06/14	14:10:9.70	49.110	131.830	7.0	4.0	—	7	3.55	0.10	7	3.51	0.14
ISC	2003/08/16	10:58:40.78	43.813	119.658	8.8	5.8	5.9	8	5.85	0.41	8	5.85	0.38
ISC	2003/10/07	15:27:27.80	45.240	133.597	49.4	4.5	4.8	8	4.36	0.21	8	4.38	0.20
ISC	2003/10/09	15:53:29.88	41.435	125.982	8.0	—	3.9	8	3.68	0.17	8	3.63	0.17
BJI	2003/10/10	13:34:27.80	41.430	125.650	15.0	—	3.7	8	3.18	0.19	8	3.12	0.19
ISC	2004/03/24	01:53:47.50	45.349	118.209	18.0	5.8	6.2	8	5.86	0.23	8	5.87	0.24
NEIC	2004/09/16	17:14:37.47	45.137	131.727	10.0	3.9	—	8	3.86	0.16	8	3.84	0.16
NEIC	2004/12/16	18:59:14.60	41.804	127.979	10.0	4.0	—	8	4.16	0.15	8	4.15	0.16
NEIC	2005/07/06	23:10:16.68	48.295	131.473	10.0	4.3	—	7	4.27	0.15	7	4.27	0.14
NEIC	2005/07/25	15:43:41.14	46.827	125.058	47.7	5.0	—	7	5.37	0.21	7	5.41	0.21
NEIC	2005/09/19	03:27:53.20	49.878	121.003	10.0	4.9	—	6	4.95	0.23	6	4.92	0.21
NEIC	2006/03/31	12:23:17.86	44.624	124.122	10.0	4.9	—	7	4.98	0.39	7	4.98	0.40
NEIC	2006/05/03	00:26:37.50	48.783	121.049	35.4	3.7	—	6	4.29	0.30	6	4.28	0.29
NEIC	2006/10/09	01:35:28.00	41.294	129.094	0.0	4.2	—	8	3.93	0.09	8	3.93	0.10
NEIC	2006/11/03	06:21:39.28	43.469	119.558	10.0	4.7	—	7	4.49	0.19	7	4.51	0.23

*Number of stations used to calculate network magnitude.
†Beijing regional network.
‡Sakhalin regional network.

Table 3

Magnitude Residuals and Station Corrections

Station		MDJ	CN2	SNY	INCN	BNX	DL2	BJT	HIA	Average
$m_b(Lg, TP)$	Correction	0.113	−0.007	0.075	−0.031	0.041	−0.183	0.056	−0.068	−0.001
	Number of events	23	23	21	22	22	21	21	21	
$m_b(Lg, \text{rms})$	Correction	0.120	−0.010	0.083	−0.051	0.045	−0.193	0.050	−0.054	−0.001
	Number of events	23	23	21	22	22	21	21	21	

Table 4

Magnitude and Yield Estimations Using the Third Peak and rms Amplitudes of Lg Waves

			Measured $A(\Delta)$ (μm)			$A(10)$ (μm)		$m_b(Lg)$		Corrected $m_b(Lg)$		Yield (kt)	
Number	Station	Distance (km)	*TP*	rms	Measured $f(Lg)$	*TP*	rms	*TP*	rms	*TP*	rms	*TP*	rms
1	MDJ	371.6	0.209	0.094	1.186	10.381	8.555	3.975	3.978	3.862	3.858	0.41	0.41
2	CN2	411.9	0.140	0.060	1.316	9.144	7.246	3.920	3.906	3.926	3.915	0.47	0.46
3	SNY	467.9	0.165	0.075	1.266	13.421	11.636	4.086	4.112	4.011	4.028	0.58	0.60
4	INCN	475.4	0.092	0.037	1.211	7.428	5.584	3.830	3.793	3.861	3.844	0.41	0.39
5	BNX	514.0	0.101	0.044	1.285	10.218	8.559	3.968	3.978	3.927	3.934	0.48	0.48
6	DL2	693.4	0.047	0.020	1.196	8.861	7.425	3.906	3.917	4.089	4.110	0.69	0.72
7	BJT	1106.2	0.014	0.005	1.011	7.246	6.369	3.819	3.850	3.763	3.800	0.33	0.35
8	HIA	1152.6	0.015	0.005	0.999	8.702	6.810	3.898	3.879	3.966	3.933	0.52	0.48
		Network-averaged value				9.425	7.773	3.925	3.926	3.926	3.928	0.49	0.49
		Standard deviation				1.970	1.861	0.086	0.097	0.100	0.101	0.11	0.12
		Yield from network magnitude								3.926	→	0.47	
											3.928	→	0.48

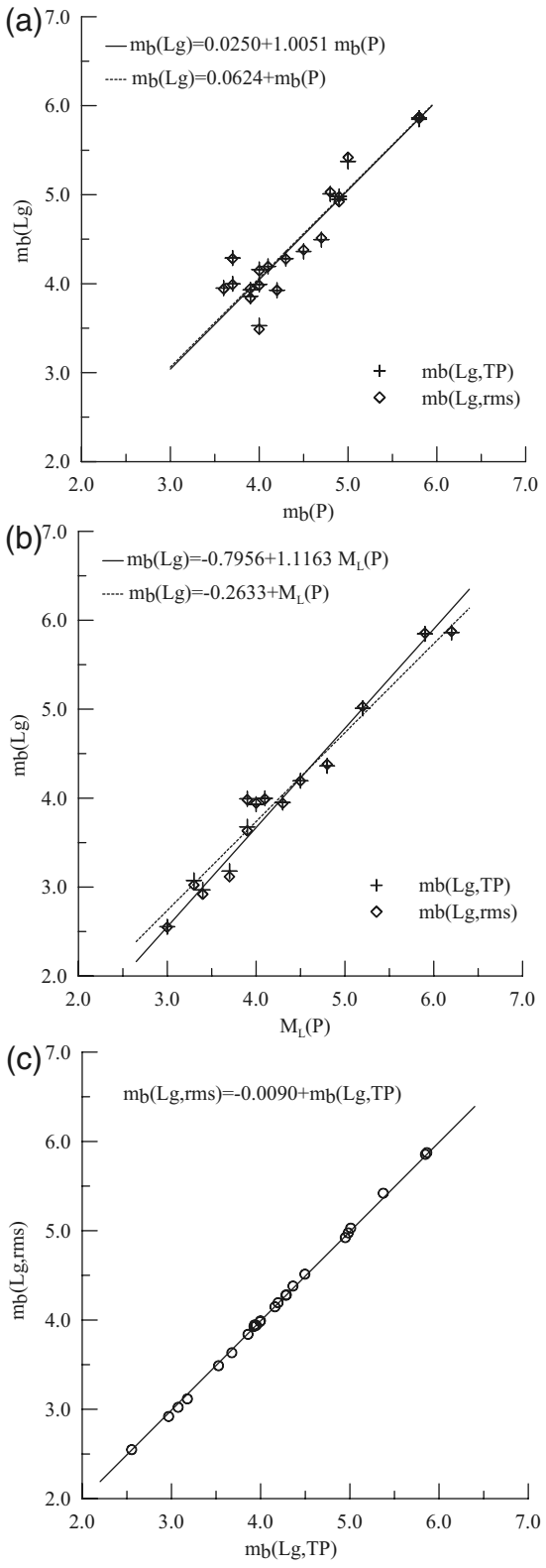

Figure 7. Comparisons between magnitudes calculated using different methods for all 24 regional events listed in Table 2 with (a) $m_b(Lg)$ versus $m_b(P)$, (b) $m_b(Lg)$ versus M_L, and (c) $m_b(Lg, \text{rms})$ versus $m_b(Lg, TP)$. In (a) and (b), crosses are for $m_b(Lg, TP)$, and circles are for $m_b(Lg, \text{rms})$. The solid lines are for least-squares fittings, and dashed lines are results with fixed unit slope.

propriate m_b-yield relationship for fully coupled nuclear explosions in a stable region such as the East Kazakhstan test site is

$$m_b = 4.45 + 0.75 \log Y. \tag{8}$$

Bowers *et al.* (2001) indicated that the *Pn*-wave speed beneath the Novaya Zemlya region is 8.05 km/sec, which is lower than the value of 8.3 km/sec beneath the East Kazakhstan region. Considering that a lower *Pn* speed is empirically an indicator of attenuation of a teleseismic *P* wave within the upper mantle, they adjusted the coefficient in equation (8) from 4.45 to 4.25 and proposed a modified m_b-yield relation for the Novaya Zemlya region. To extend the magnitude-yield relation to smaller events, they further argued that the slop of 0.75 in equation (8) is a consequence of detonating the explosions at a scaled depth of burial. By reasonably assuming that there is a minimum depth for fully coupled explosions and choosing this depth as the scaled depth for a 1 kt explosion, Bowers *et al.* (2001) obtained a modified equation for the fully coupled explosion

$$m_b = 4.25 + 0.75 \log Y \quad \text{for } Y \geq 1 \text{ kt}, \tag{9a}$$

$$m_b = 4.25 + \log Y \quad \text{for } Y < 1 \text{ kt}. \tag{9b}$$

Illustrated in Figure 8 are magnitude-yield relations for equations (7)–(9). The observations that support these magnitude-yield relations are roughly $4.5 \leq m_b \leq 6.5$. These relations give similar yield estimates for events of *M* 5 or larger, but their predictions are scattered for events with magnitudes smaller than 4.

To apply the magnitude-yield relation from a calibrated region to an uncalibrated area, proper assumptions must be made. The Northeast China–North Korea region is covered by continental crust (Zhang *et al.*, 2002; Li and Yuan, 2003). The geology map (Institute of Geology, State Academy of Sciences, Democratic People's Republic of Korea, 1996) shows that the Korean Peninsula largely consists of Precambrian rocks. The surface geology map shown in Figure 9 illustrates that the region surrounding the NKTS (indicated with a star) is mainly composed of three types of rocks: Prophyritic biotite granite, fine-grained granite, and diorite. The crustal *Lg* attenuation tomography (Xie *et al.*, 2006) found this region has a relatively high and uniform *Q*-value. The estimated *Pn*-wave speed beneath this region varies between 7.4 and 8.0 km/sec (Marshall *et al.*, 1979; Zhang *et al.*, 2002). These results suggest that the NKTS is likely a hard-rock site in an area with stable continental crust.

Because of the scatter of these empirical relations at lower magnitudes, we further investigate these relations by comparing them with a group of small chemical explosions with known yields. In August 1998, a group of chemical explosions with nominal yields between 1.0 and 2.0 tons were detonated on the China–North Korea border and were re-

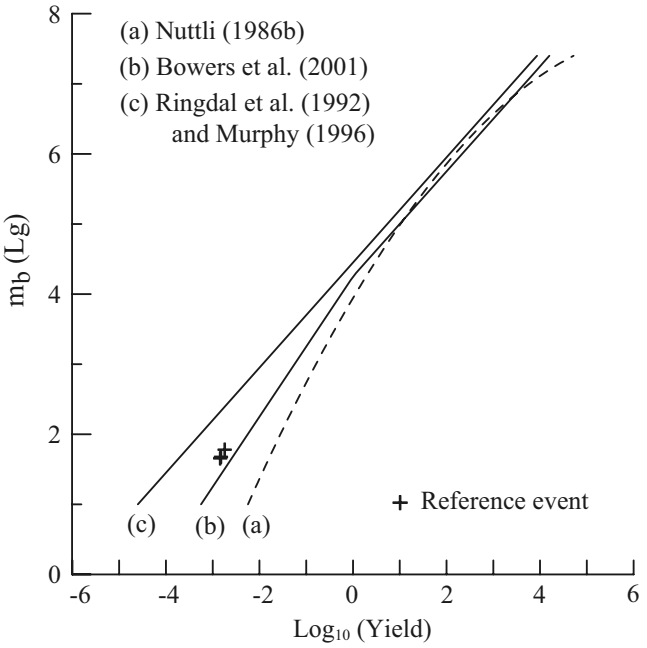

Figure 8. Empirical magnitude-yield relations from (a) Nuttli (1986b), (b) Bowers *et al.* (2001), and (c) Ringdal *et al.* (1992) and Murphy (1996). The three chemical explosions with known yields are illustrated with crosses.

corded on four GSN stations: MDJ, HIA, BJT, and INCN. These chemical explosions were originally for refraction seismic investigation (Zhang *et al.*, 2002) and have been used by Salzberg and Marshall (2007) for calibrating the North Korean test. These explosions were detonated in boreholes with steel casings. The source parameters of these explosions including their locations, nominal yields, and source depths were provided by X.-K. Zhang (personal comm., 2008) and are listed in Table 5. The locations of these chemical explosions are indicated in Figure 1 as open stars. Using the same method for processing the North Korean test and earthquakes, we calculated their regional magnitudes $m_b(Lg, TP)$ and $m_b(Lg, \text{rms})$, which are also listed in Table 5. The magnitude versus yield points for these chemical explosions are illustrated in Figure 8 along with different empirical relations. Although 2–3 orders of magnitude smaller than the North Korean nuclear explosion, these small chemical explosions still provide constraints on the empirical relations. It appears that the chemical explosion data favor the fully coupled relations by Ringdal *et al.* (1992), Murphy (1996), and Bowers *et al.* (2001), while Nuttli's (1986b) relation may overestimate the yield in this region.

Based on the geological properties in the Korean Peninsular and Northeast China region and the magnitude-yield relations of these chemical explosions, we first use the modified equation (9) by Bowers *et al.* (2001) to estimate the yield of the North Korean test. The original consideration of Bowers *et al.* (2001) was to use this relation for correcting the regional variation of teleseismic m_b in the Novaya Zemlya region. However, because our $m_b(Lg)$ has not been directly compared with the magnitude system of Ringdal *et al.* (1992) and Murphy (1996), equation (9) may also be suitable for the North Korea–Northeast China region. In Table 4, the yields for individual stations are calculated from station magnitudes. The network-averaged yield is then calculated from these station values. The average yield is 0.49 kt for both $m_b(Lg, TP)$ and $m_b(Lg, \text{rms})$, and the standard deviation is approximately 0.1 kt. We also calculate the yield directly from the network magnitude. The value is 0.47 kt for $m_b(Lg, TP)$ and 0.48 kt for $m_b(Lg, \text{rms})$ (see Table 4). If we use the original magnitude-yield relation by Ringdal *et al.* (1992) and Murphy (1996) but keep the assumption that the explosion has a minimum burial depth, which is the scaled depth for a 1-kt explosion, then the yield for the North Korean nuclear test is 0.30 kt for both $m_b(Lg, TP)$ and $m_b(Lg, \text{rms})$.

P/S Spectral Ratios and Event Discrimination

Figures 3 and 4 show broadband seismograms for the 9 October 2006 North Korean nuclear explosion and an earthquake that occurred on 16 April 2002 near the NKTS. As we have mentioned, because it is a dislocation source, the earthquake radiates strong *S* waves, while the explosion source generates more *P* waves. This forms the basis for explosion source identification using P/S-type spectral ratios.

We select four regional earthquakes close to the NKTS (events 20031010, 20020416, 20020505, and 20041216, all listed in Table 2) and compare their spectral ratios with the North Korean explosion. The vertical-component seismograms from these earthquakes and the nuclear explosion are used to calculate spectra for regional waves. The following group velocity windows are used for different phases: *Pn*, 7.8–6.4 km/sec; *Pg*, 6.3–5.1 km/sec; *Sn*, 4.6–4.0 km/sec; and *Lg*, 3.7–2.9 km/sec. First, the instrument responses are deconvolved from the seismograms and then the displacement Fourier spectra are calculated. The pre-*P* noise is removed using a method similar to that used for calculating the regional magnitude, but the noise from the coda waves of other phases is neglected. A 20% cosine taper is used for all Fourier transforms. Illustrated in Figure 10 are typical spectra from selected phases and stations for the North Korean nuclear explosion and earthquake 20020416 near the NKTS. The blue, red, and black lines are for *P*-type spectra, *S*-type spectra, and noise, respectively. Note that the left-hand column is for the explosion and the right-hand column is for the earthquake. The spectra show generally good signal-to-noise ratios except at low- and high-frequency ends. Figure 11 shows logarithmic spectral ratios of Pg/Lg, Pn/Lg, and Pn/Sn (gray lines) and their smoothed values (solid circles) for phases and stations similar to those shown in Figure 10. We set a threshold signal-to-noise ratio of 1.8 for both *P*- and *S*-type waves, below which the spectral ratios are dropped. In Figure 11, at frequencies for which the

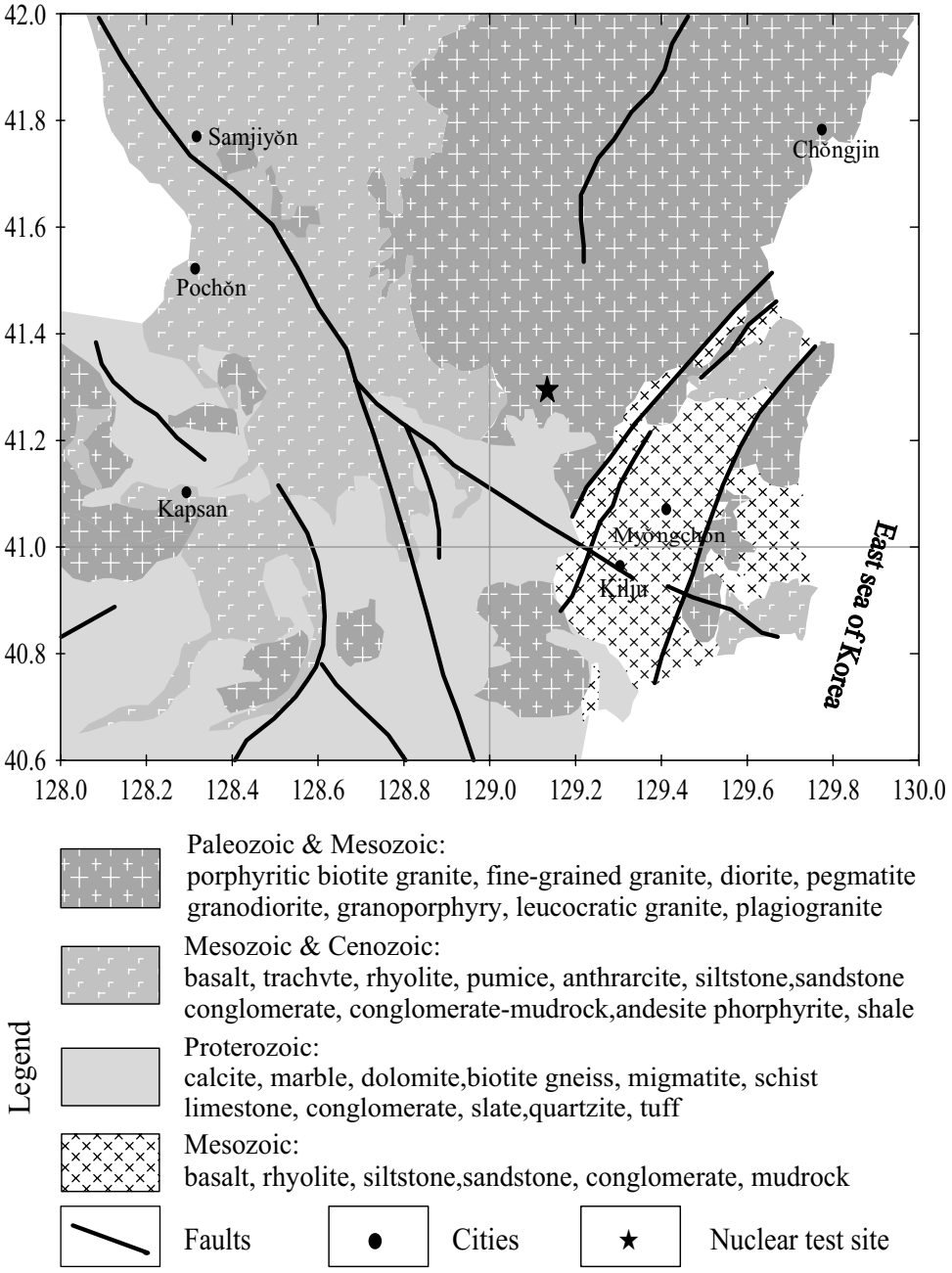

Figure 9. Surface geology map near the NKTS (Institute of Geology, State Academy of Sciences, Democratic People's Republic of Korea, 1996).

Table 5

Source Parameters for Three Chemical Explosions

Date (yyyy/mm/dd)	Time (UTC)	Latitude (°N)	Longitude (°E)	Depth (m)	Yield (ton)	$m_b(Lg, TP)$	$m_b(Lg, \text{rms})$
1998/08/12	15:00:08.18	42.865	128.223	7.4	1.50	1.665	1.689
1998/08/18	14:00:06.69	42.914	129.324	11.4	1.80	1.776	1.786
1998/08/19	15:00:07.79	42.091	128.739	28.8	1.45	1.656	1.657

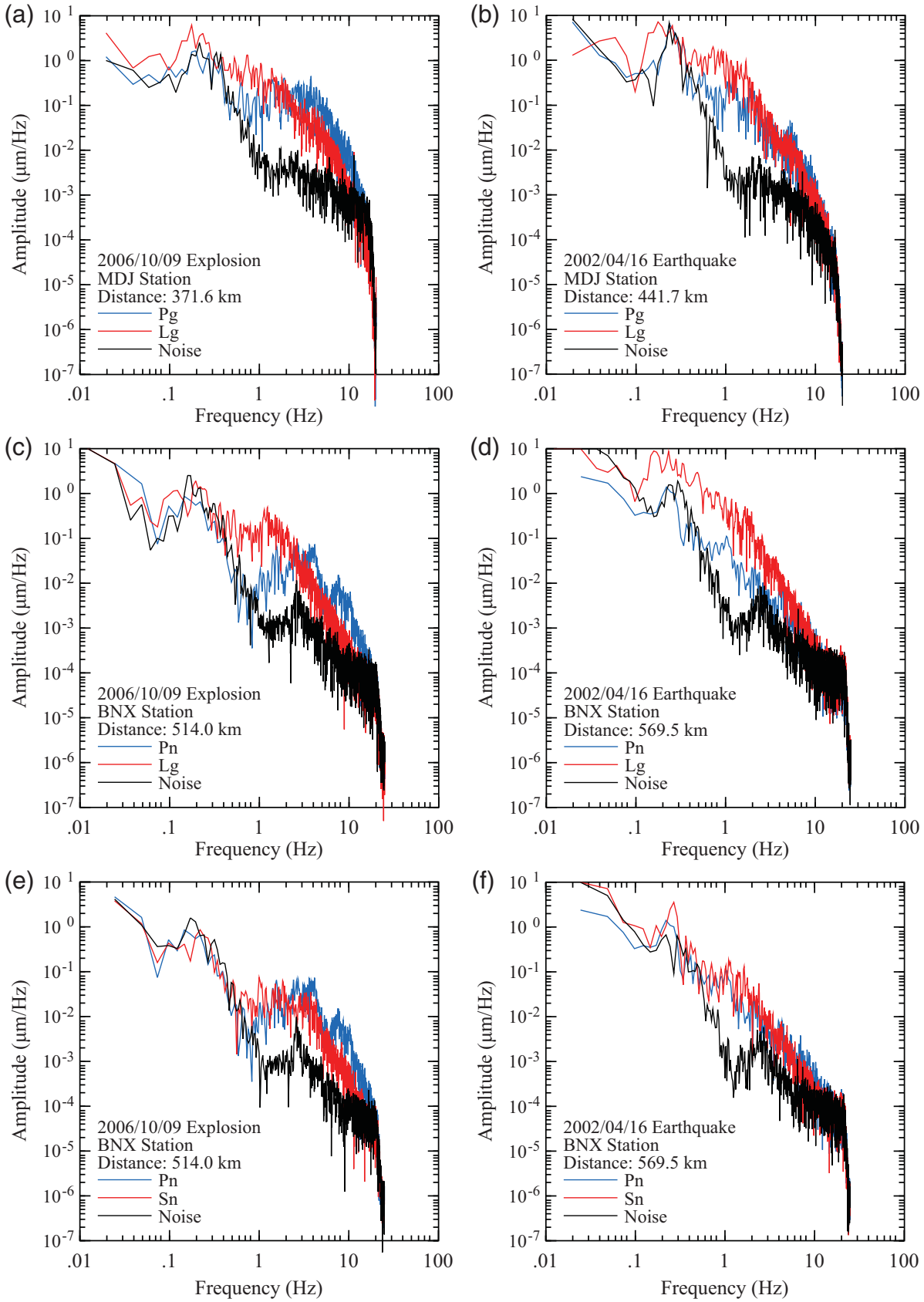

Figure 10. Typical *Pn*, *Sn*, *Pg*, *Lg*, and noise spectra from selected stations. The left-hand column is for the North Korean nuclear explosion, and right-hand column is for the earthquake 20020416. The blue lines are for *P*-type waves, the red lines are for *S*-type waves, and the black lines are for noise.

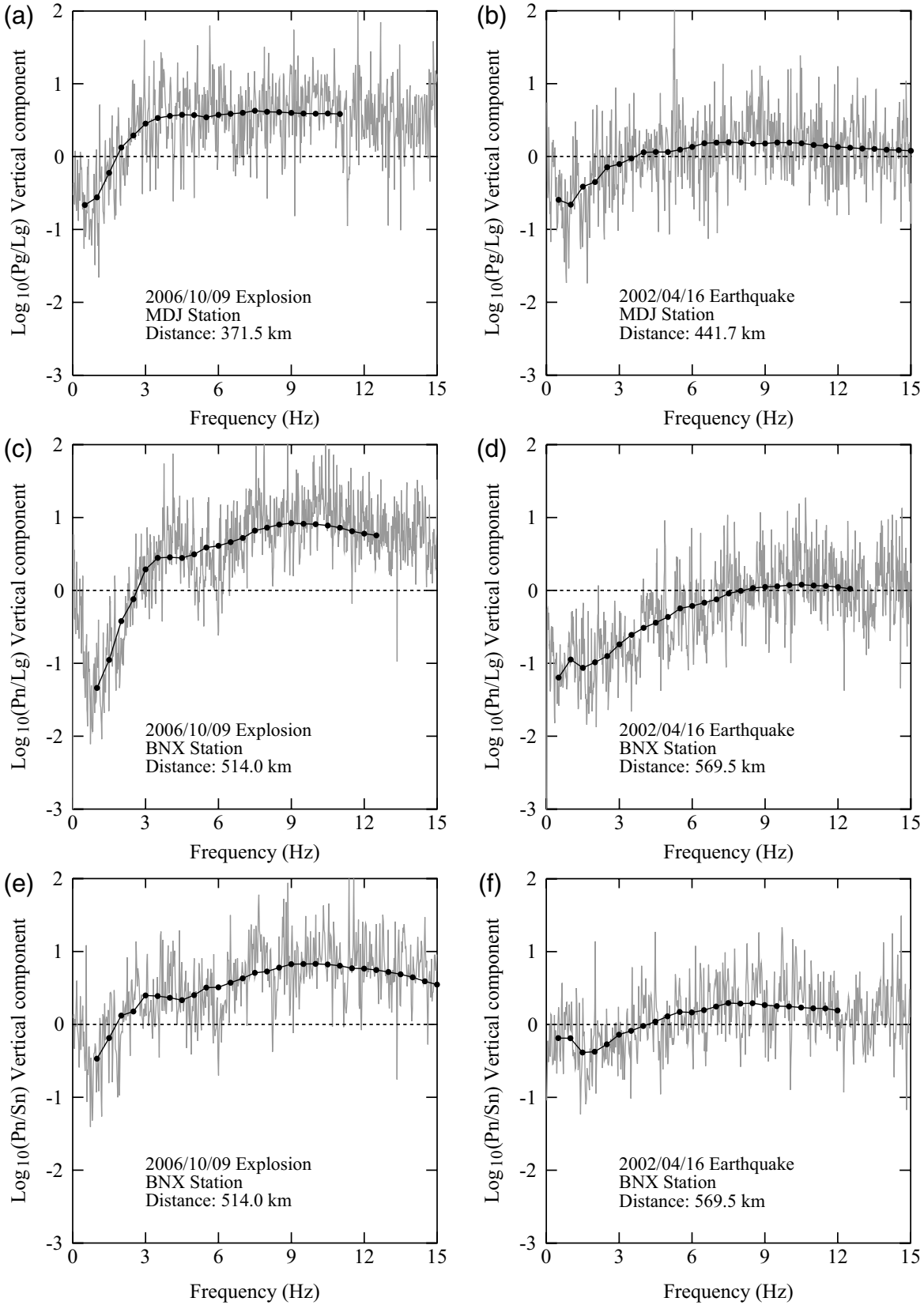

Figure 11. The logarithmic spectral ratios Pg/Lg, Pn/Lg, and Pn/Sn (gray lines) and their smoothed values (solid circles) for stations and phases similar to those shown in Figure 10. Note that the left-hand column is for the North Korean nuclear explosion and the right-hand column is for the earthquake. At frequencies where the smoothed spectral ratios are not shown, the data have been dropped due to their low signal-to-noise ratios.

smoothed spectral ratios are not shown, the data have been dropped. The log average is used in these calculations, and the frequency band used for smoothing is between $f/\sqrt{2}$ and $\sqrt{2}f$ (Bowman and Kennett, 1991; Hartse *et al.*, 1997; Yang, 2002; Richards and Kim, 2007). The explosion and the earthquake have very similar propagation paths, but the former has P/S-type ratios that, at above 2 Hz, are apparently higher than those from the latter.

Using the network-averaged ratios from a group of stations can effectively reduce the fluctuations from individual observations, building a robust discriminant. The observed spectral ratios are composed of the information of excitation spectra from different regional phases and can be used to characterize the sources. However, the spectral ratios are also affected by the distance-dependent geometrical spreading and attenuation; thus, proper distance correction may be required (Hartse *et al.*, 1997). To check this distance dependence, we use spectral ratios from four earthquakes to calculate their distance dependence. Figure 12 shows the Pg/Lg, Pn/Lg, and Pn/Sn spectral ratios versus distance for selected frequencies. At each frequency, a slope is calculated using linear regressions. In general, the low-frequency ratios have apparent distance dependence and large correlations. At high frequencies, the signals are more depleted at stations with longer distances, and the correlations become unapparent. We choose a reference distance of 500 km and use the calculated slopes to correct all spectral ratios before summing them together to give the network-averaged ratios. The station site effects may also affect the spectral-ratio measurement. However, the current data set does not permit us to calculate a broadband site correction for spectral ratios; thus, it is neglected here.

Figure 13 shows the Pg/Lg, Pn/Lg, and Pn/Sn spectral ratios for all eight stations in the network with different symbols for each station. The left-hand column is for the nuclear explosion and the right-hand column is for earthquake 20020416. The measurements have been distance corrected and smoothed. Although the spectral ratios demonstrate a general tendency for the explosion source to have higher ratios than the earthquake, measurements from individual stations show large scatter and some overlap between the explosion and the earthquake populations. After taking the average, the network values of these ratios are illustrated in Figure 13 with solid lines.

The left-hand column in Figure 14 shows network-averaged Pg/Lg, Pn/Lg, and Pn/Sn spectral ratios for five events in the investigated region including the nuclear explosion and four earthquakes (all listed in Table 2 and Fig. 1). The network-averaged spectral ratios clearly separate the explosion from the earthquakes at all frequencies above 2.0 Hz. On the right-hand side of Figure 14, histograms show the differences between the spectral ratios of the explosion and the maximum spectral ratios from earthquakes. Again, the separation is apparent.

Discussion and Conclusions

Based on regional observations from broadband digital seismic stations located in Northeast China and South Korea, we investigate the seismic characteristics of the 9 October 2006 North Korean nuclear test. The stations range between 371 and 1153 km from the test site. Broadband regional data from the nuclear test and a group of regional earthquakes were recorded between December 2000 and November 2006. We first use these events to calibrate the Lg-wave magnitude in the network. Both the $m_b(Lg, TP)$ and $m_b(Lg, \mathrm{rms})$ are calculated, and station corrections are determined. Comparing the Lg magnitude with the global body-wave magnitude reported from NEIC, ISC, BJI, and SKHL, both methods show consistent results with the global magnitude m_b. The calibrated network is then used to calculate the regional magnitude of the North Korean nuclear test yielding $m_b(Lg)$ 3.93. Investigating a group of chemical explosions conducted in this region and considering the geological properties of the investigated area, the fully coupled magnitude-yield relations by Ringdal *et al.* (1992), Murphy (1996), and Bowers *et al.* (2001) appear to give close estimates for the yield of the North Korean explosion, while Nuttli's (1986b) relation may overestimate the yield. The yield calculated using the modified relation by Bowers *et al.* (2001) is 0.48 kt. If using the equation by Ringdal *et al.* (1992) and Murphy (1996), assuming a minimum burial depth that is the scaled depth for a 1 kt explosion, the estimated yield is about 0.30 kt.

Even with these considerations and assumptions, estimating the yield in an uncalibrated region still involves big uncertainties. The empirical magnitude-yield relations are not always portable. Most of these relations are obtained from large magnitude events. Extrapolating them to low-yield events should be done very carefully, and the relation is not necessarily linear. Considering the low yield of the North Korean nuclear test, its scaled depth is less than 100 m. It is likely this explosion is significantly overburied, and the depth variation is a big source of uncertainty in yield estimation (Bowers *et al.* 2001; Herrmann *et al.* 2007; Koper *et al.* 2008). Based on the preceding consideration, our yield estimate for the North Korean nuclear explosion is preliminary, and efforts to estimate the actual burial depth will better constrain the yield.

Compared to earthquake data, the 9 October 2006 event shows typical features of an explosion, including a stronger P phase, a relatively weak S phase, and a clear SP Rg wave. The P/S-type spectral ratios between different regional phases, for example, Pg/Lg, Pn/Lg, and Pn/Sn, were calculated for both the explosion and a group of earthquakes close to the test site. These spectral ratios show a general feature that the explosion has a higher spectral ratio compared to those from earthquakes. To remove large scatter from observations at individual stations, we calculate the network average for these amplitude ratios. For frequencies above 2.0 Hz, all three network-averaged spectral ratios of

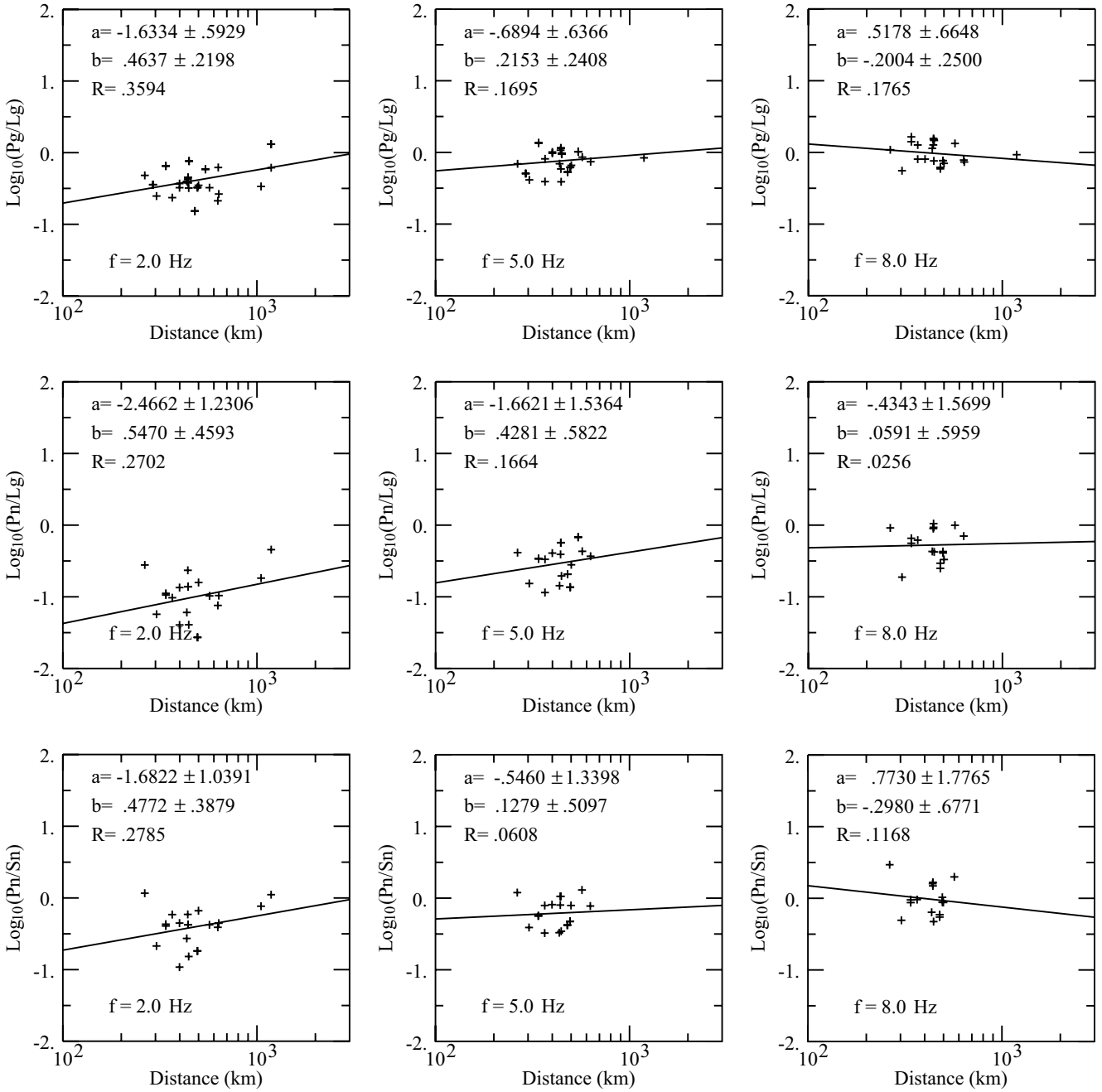

Figure 12. Spectral ratios Pg/Lg, Pn/Lg, and Pn/Sn versus distances for frequencies 2.0, 5.0, and 8.0 Hz. At each frequency, a linear regression is used to determine the distance dependence of the observed spectral ratios.

the 9 October 2006 explosion are completely separated from the similar ratios of regional earthquakes.

Similar results have been reported by other authors. Kim and Richards (2007) and Richards and Kim (2007) reported the Pg/Lg spectral ratios recorded at station MDJ. Their results showed that the North Korean explosion is well separated from the earthquakes for frequencies above 3 Hz. However, for a group of small chemical explosions, the spectral ratios overlapped between frequencies 1 and 7 Hz but were fairly well separated at 9 Hz and above. Koper *et al.* (2008) compared the amplitude ratios Pn/Lg and Pg/Lg for 1–4 Hz signals at station MDJ. They found the explosion always had the highest ratios, and the separation of the explosion from the earthquake population increased as the frequency was increased. Walter *et al.* (2007) reported Pg/Lg spectral ratios at 1–2, 2–4, 4–6, and 6–8 Hz from stations MDJ and TJN. They found that MDJ discriminated the explosion and earthquakes at all frequencies above 2 Hz. The results from the TJN showed partial overlap at low frequencies but discriminated well at frequencies of 6–8 Hz. These

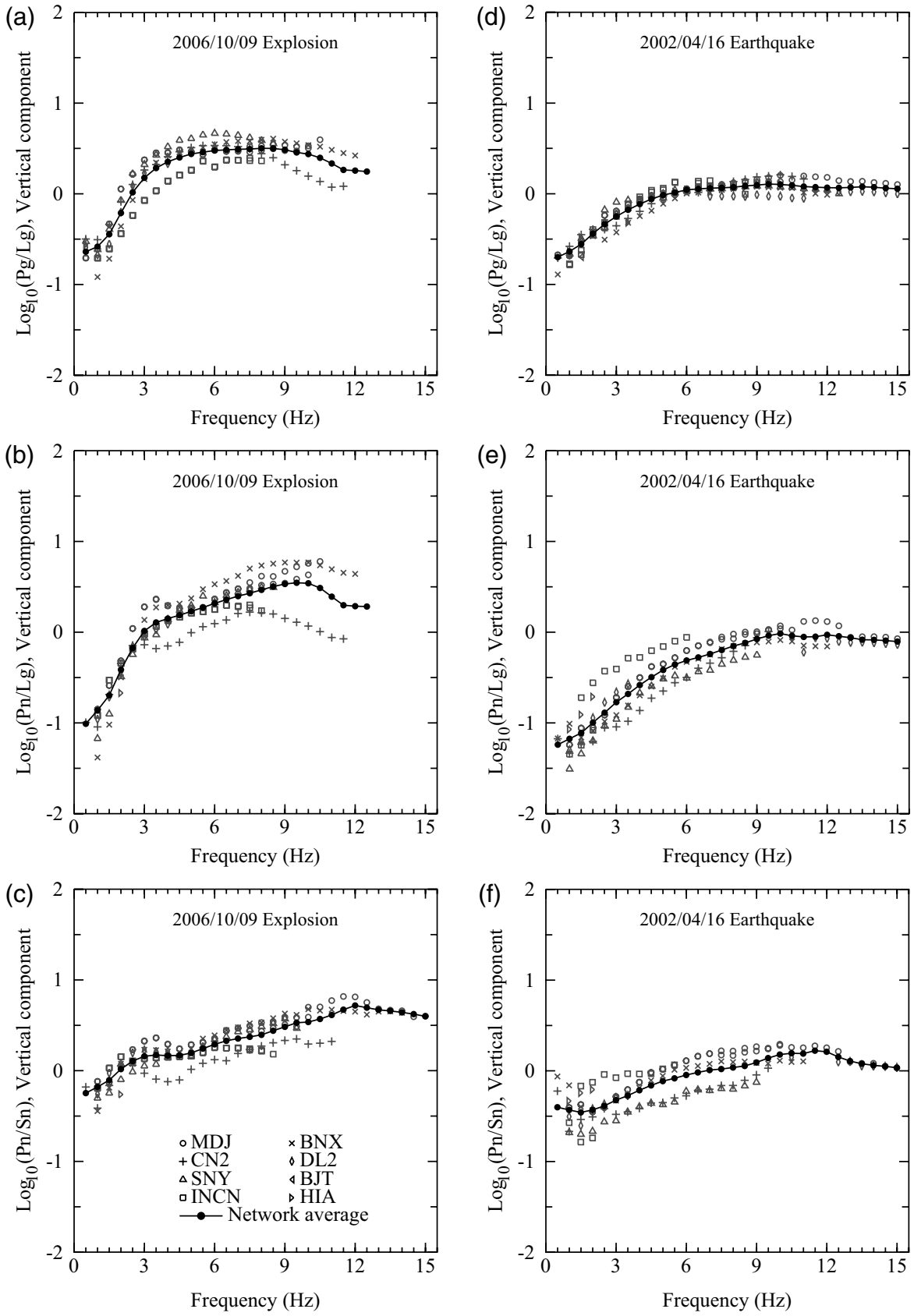

Figure 13. P/S-type spectral ratios for Pg/Lg, Pn/Lg, and Pn/Sn from all eight stations and their network-averaged values. The left-hand column is for the North Korean nuclear explosion, and right-hand column is for earthquake 20020416.

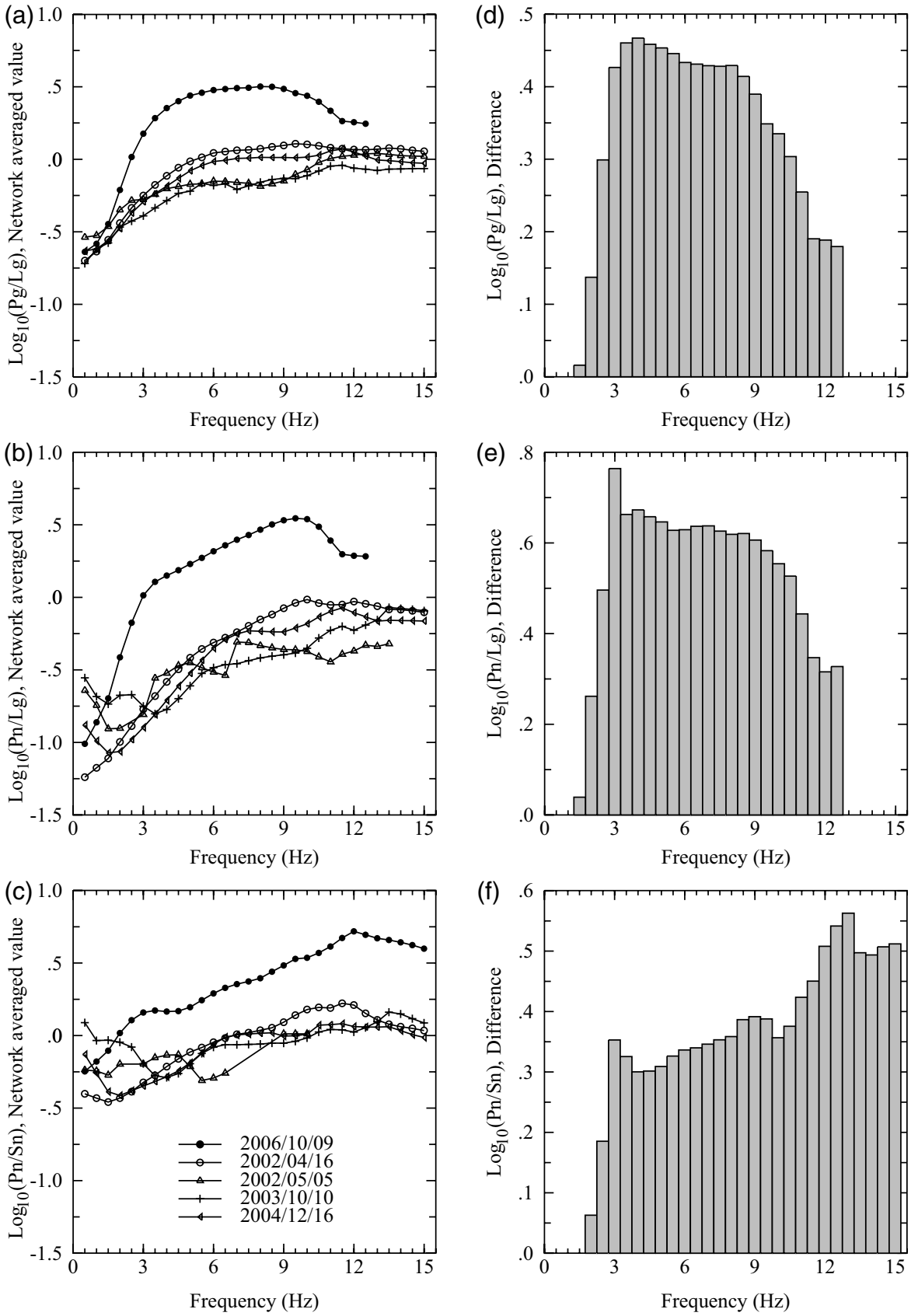

Figure 14. The left-hand column illustrates the network-averaged spectral ratios for Pg/Lg, Pn/Lg, and Pn/Sn from five regional events including the North Korean nuclear explosion and four nearby earthquakes (all listed in Table 2). In the right-hand column are histograms showing differences between spectral ratios from the explosion and the maximum spectral ratios from all earthquakes.

results show the North Korean nuclear explosion has distinct features that differ from earthquakes and suggest that any well-coupled single-shot explosion with yield similar to the North Korean test detonated in this region has a large chance of being detected and identified by a high-quality regional network similar to the one used in this study.

Data and Resources

Waveforms recorded at the GSN stations used in this study were collected from the Incorporated Research Institutions for Seismology (IRIS) Data Management Center at www.iris.edu (last accessed June 2008). The data recorded by CNDSN stations were from the China Earthquake Network Center (CENC). Inquiries regarding the availability of these data may be sent to this agency. The source parameters of three chemical explosions were provided by Xian-Kang Zhang. Some figures were made using the Generic Mapping Tools version 4.3.1 (www.soest.hawaii.edu/gmt, last accessed May 2008).

Acknowledgments

The authors wish to thank Bill Walter and another anonymous reviewer for valuable comments. We thank Thorne Lay and Howard Patton for many discussions on this work. This research is supported by the Chinese Academy of Sciences (Grant Number CXJJ -225) and the National Natural Science Foundation of China (Grant Number 90714012). One of us, X.-B.X., wishes to thank the Air Force Research Laboratory (AFRL) for support under Grant Number FA8718-05-C-0021.

References

Ai, Y., T. Zheng, Y. He, and D. Dong (2003). A complex 660 km discontinuity beneath northeast China, *Earth Planet. Sci. Lett.* **212,** 63–71.

Bowers, D., P. D. Marshall, and A. Douglas (2001). The level of deterrence provided by data from the SPITS seismometer array to possible violations of the comprehensive test ban in the Novaya Zemlya region, *Geophys. J. Int.* **146,** 425–438.

Bowman, J. R., and B. L. N. Kennett (1991). Propagation of *Lg* waves in the North Australian Craton: influence of crustal velocity gradients, *Bull. Seismol. Soc. Am.* **81,** 592–610.

Fisk, M. D. (2006). Source spectral modeling of regional P/S discriminants at nuclear test sites in China and the former Soviet Union, *Bull. Seismol. Soc. Am.* **96,** 2348–2367, doi 10.1785/0120060023.

Fisk, M. D., H. L. Gray, and G. D. McCartor (1996). Regional discrimination without transporting thresholds, *Bull. Seismol. Soc. Am.* **86,** 1545–1558.

Ge, H., Y. Ni, C. Huang, J. Li, Y. Li, Y. Jiang, and F. Lu (1989). *Lg* velocity, attenuation and magnitude of the continent area in China, *Chin. Sci. Bull.* **24,** 1889–1892 (in Chinese).

Hansen, R. A., F. Ringdal, and P. G. Richards (1990). The stability of rms *Lg* measurements and their potential for accurate estimation of the yields of Soviet underground nuclear explosions, *Bull. Seismol. Soc. Am.* **80,** 2106–2126.

Hartse, H. E., S. R. Taylor, W. S. Scott, and G. E. Randall (1997). A preliminary study of regional seismic discrimination in central Asia with emphasis in western China, *Bull. Seismol. Soc. Am.* **87,** 551–568.

Herrmann, R. B., W. R. Walter, and M. E. Pasyanos (2007). Seismic source and path calibration in the Korean peninsula, Yellow sea and Northeast China, *29th Monitoring Research Review: Ground-Based Nuclear Explosion Monitoring Technologies*, 592–601.

Huang, C., Z. Gao, L. Shi, and Y. Ni (1990). *Lg* wave attenuation and magnitude in Northeast China region, *Northeast. Seismol. Res.* **6,** 41–49 (in Chinese).

Institute of Geology, State Academy of Sciences, Democratic People's Republic of Korea (1996). *Geology of Korea*, Jun, P. R., K. H. Gap and J. G. Pu (Editors), Foreign Languages Books Publishing House, Pyongyang, 382 pp.

Israelsson, H. (1992). RMS Lg as a yield estimator in Eurasia, Final Technical Report PL-TR-92-2117(I), Phillips Laboratory, Hanscom Air Force Base, Massachusetts.

Kim, W.-Y., and P. G. Richards (2007). North Korean nuclear test: seismic discrimination at low yield, *EOS Trans. AGU* **88,** 158–161.

Koper, K. D., R. B. Herrmann, and H. M. Benz (2008). Overview of open seismic data from the North Korea event of 9 October 2006, *Seism. Res. Lett.* **79,** 178–185.

Li, X., and X. Yuan (2003). Receiver functions in northeast China: implications for slab penetration into the lower mantle in Northwest Pacific subduction zone, *Earth Planet. Sci. Lett.* **216,** 679–691.

Marshall, P. D., D. L. Springer, and H. C. Rodean (1979). Magnitude corrections for attenuation in the upper mantle, *Geophys. J. R. Astron. Soc.* **57,** 609–638.

Murphy, J. R. (1996). Type of seismic events and their source descriptions, in *Monitoring a Comprehensive Test Ban Treaty*, E. Husebye and A. M. Dainty (Editors), Springer, New York, 247–293.

Nuttli, O. W. (1973). Seismic wave attenuation and magnitude relations for eastern North America, *J. Geophys. Res.* **78,** 876–885.

Nuttli, O. W. (1980). The excitation and attenuation of seismic crustal phases in Iran, *Bull. Seismol. Soc. Am.* **70,** 469–485.

Nuttli, O. W. (1986a). Yield estimates of Nevada Test Site explosions obtained from seismic *Lg* waves, *J. Geophys. Res.* **91,** 2137–2151.

Nuttli, O. W. (1986b). *Lg* magnitudes of selected East Kazakhstan underground explosions, *Bull. Seismol. Soc. Am.* **76,** 1241–1251.

Patton, H. J. (1988). Application of Nuttli's method to estimate yield of Nevada test site explosions recorded on Lawrence Livermore National Laboratory's digital seismic system, *Bull. Seismol. Soc. Am.* **78,** 1759–1772.

Patton, H. J. (2001). Regional magnitude scaling, transportability, and Ms:mb discrimination at small magnitudes, *Pure Appl. Geophys.* **158,** 1951–2015.

Patton, H. J., and J. Schlittenhardt (2005). A transportable mb(Lg) scale for central Europe and implications for low-magnitude Ms–mb discrimination, *Geophys. J. Int.* **163,** 126–140.

Priestley, K. F., and H. J. Patton (1997). Calibration of $m_b(Pn)$, $m_b(Lg)$ scales and transportability of the M_0:m_b discriminant to new tectonic regions, *Bull. Seismol. Soc. Am.* **87,** 1083–1099.

Richards, P. G., and W.-Y. Kim (2007). Seismic signature, *Nat. Phys.* **3,** 4–6.

Ringdal, F., P. D. Marshall, and R. W. Alewine (1992). Seismic yield determination of Soviet underground explosions at the Shagan River test site, *Geophys. J. Int.* **109,** 65–77.

Salzberg, D., and M. Marshall (2007). Seismic source locations and parameters for sparse networks by matching observed seismograms to semi-empirical synthetic seismograms: Applications to Lop Nor and North Korea, *29th Monitoring Research Review: Ground-Based Nuclear Explosion Monitoring Technologies*, 472–481.

Schlittenhardt, J. (2001). Teleseismic *Lg* of Semipalatinsk and Novaya Zemlya nuclear explosions recorded at the GRF (Gräfenberg) array: comparison with regional *Lg* (BRV) and their potential for accurate yield estimation, *Pure Appl. Geophys.* **158,** 2253–2274.

Taylor, S. R., M. D. Denny, E. S. Vergino, and R. E. Glaser (1989). Regional discrimination between NTS explosions and western U.S. earthquakes, *Bull. Seismol. Soc. Am.* **79,** 1142–1176.

Walter, W. R., E. Matzel, M. E. Pasyanos, D. B. Harris, R. Gok, and S. R. Ford (2007). Empirical observations of earthquake-explosion discrimination using P/S ratios and implications for the sources of explosion S-waves, *29th Monitoring Research Review: Ground-Based Nuclear Explosion Monitoring Technologies*, 684–693.

Walter, W. R., K. Mayeda, and H. J. Patton (1995). Phase and spectral ratio discrimination between NTS earthquakes and explosions, part 1: Empirical observations, *Bull. Seismol. Soc. Am.* **85,** 1050–1067.

Xie, J. (2002). Source scaling of *Pn* and *Lg* spectra and their ratios from explosions in central Asia: implications for the identification of small seismic events at regional distances, *J. Geophys. Res.* **107,** no. B7, 2128, doi 10.1029/2001JB000509.

Xie, J., Z. Wu, R. Liu, D. Schaff, Y. Liu, and J. Liang (2006). Tomographic regionalization of crustal Lg Q in eastern Eurasia, *Geophys. Res. Lett.* **33,** L03315, doi 10.1029/2005GL024410.

Yang, X. (2002). A numerical investigation of *Lg* geometrical spreading, *Bull. Seismol. Soc. Am.* **92,** 3067–3079.

Zhang, C. K., X. K. Zhang, J. R. Zhao, B. F. Liu, J. S. Zhang, Z. X. Yang, Y. Hai, and G. W. Sun (2002). Crust-mantle structure of the Changbaishan Tianchi volcanic region and its vicinity: an exploratory study and inferences, *Chin. J. Geophys.* **45,** 862–871.

Institute of Geology and Geophysics
Chinese Academy of Sciences
19 Beituchengxilu, Chaoyang District
Beijing 100029, China
zhaolf@mail.igcas.ac.cn
(L.-F.Z., Z.-X.Y.)

Institute of Geophysics and Planetary Physics
University of California at Santa Cruz
1156 High Street
Santa Cruz, California 95064
xie@pmc.ucsc.edu
(X.-B.X.)

Institute of Tibetan Plateau Research
Chinese Academy of Sciences
18 Shuangqinglu, Haidian District
Beijing 100085, China
(W.-M.W.)

Manuscript received 18 September 2007